Biomimetic nanopore for sensitive and selective detection of Hg (II) in conjunction with single-walled carbon nanotubes

Qingfeng Zhai[a,b], Shiqi Zhang[b], Hong Jiang[b], Jiahai Wang[*a,b], Qin Wei[*a], Erkang Wang[*b]

[a]Key Laboratory of Chemical Sensing & Analysis in Universities of Shandong, School of Chemistry and Chemical Engineering, University of Jinan, Jinan, 250022, China.

[b]State Key Laboratory of Electroanalytical Chemistry, Changchun Institute of Applied Chemistry, Chinese Academy of Sciences, Changchun, Jilin,130022, China, and Graduate School of the Chinese Academy of Sciences, Beijing, 100039, China.

*Correspondence author: *jhwang@ciac.jl.cn; sdjndxwq@163.com; ekwang@ciac.jl.cn*

Homepage：http://nanopore.weebly.com

Tel: + 86-531-82767872

Fax: + 86-531-82765969

Abstract

A new method is proposed for selective detection of Hg^{2+} based on the combination of biomimetic nanopore and single-walled carbon nanotubes (SWNTs). By virture of single-walled carbon nanotubes (SWNTs), folded DNA in the presence of Hg^{2+} can be separated from single-stranded DNA. The folded DNA therefore can be quantitated with cone-shaped nanopore whose surface is coated by PEI/ Zr^{4+}. The concentration of folded DNA has linear relationship with the concentration of Hg^{2+}, allowing the metal

ion to be indirectly measured by biomimetic nanopore. Both sensitivity and selectivity based on this paradigm can be ganranteed without immobilization of probes onto the nanopore surface. This approach can warrant the detection limit for Hg^{2+} down to 8.3 nM with high selectivity against other metal ions. Moreover, this method is challenged to detect Hg^{2+} in lake water with satisfactory results. This research demonstrates an alternative approach to detect targets of interest, which holds high prospects for detecting other biomolecules or metal ions which have their own aptamer or can interact with certain DNAs having specific sequences.

Keywords： Biomimetic nanopore, Single-walled carbon nanotubes, Ion-current rectification, Hg(II) detection, Nucleic acids

1 Introduction

Until now, artificial nanopores initially inspired by biological nanopores have made a giant leap toward the bioanalysis application.[1-5] The capability of nanopore for bioanalysis relies on two methods including resistive-pulse sensing (RPS)[6,7] and ion-current rectification (ICR).[8-10] Both nanopore in thin membrane and engineered protein channel wisely adopted RPS to quantitatively detect the target of intertest. The combination of RPS and thin nanopore is highly advantageous, which has been successfully applied in many cases.[11,12] In 2008, Wang et al. applied ICR in analysis of positively hydrophobic drugs with conically shaped nanopore in kapton membrane.[13] Since then, sensor platforms based on ICR gradually came into sight.[5,14-16] More

recently, the detection of DNA[17-19], proteins[20-23], biomolecules[14,15,24-27] and metal ions[5,28-30] with cone-shaped biomimetic nanopore have been achieved.

The principle of these kinds of biosensors based on ICR is pretty straightforward and implemented via the change in the surface charge of the nanopore,[31,32] which can be monitored by current-versus-voltage (I-V) curves. All these cases entail immobilization of target-specific probes onto the nanopore surface and the immobilization is routinely accomplished by covalent bond chemistry[24] and electrostatic adsorption[33]. As compared with those robust analytical techniques[34-36], the sensitivity and selectivity are far less satisfactory. The barricade that impedes the progress is that we still lack an efficient way to engineer the nanopore surface. The ideal sensor platform based on cone-shaped nanopore must feature the property that low concentration of target can reverse the surface charge status significantly after target interacts with the probe-immobilized nanopore surface. But unfortunately, it is not always successful to find a probe whose net charge is opposite to the target of interest. Furthermore, probe immobilization brings high steric hindrance and changes the hydrophobicity of the nanopore, which is not favorable for target binding.

In the present study, a new paradigm based on cone-shaped nanopore combined with SWNTs is proposed. The Zr^{4+}-coated nanopore act as a counter which can quantitatively detect the concentration of folded DNA (or aptamer); SWNTs remove the excess single-stranded DNA (ssDNA) (or aptamer) which has not folded into duplex conformation in the presence of target.[37-39] Zirconium ion (Zr^{4+}) has strong affinity for the groups containing phosphate, which has been an ideal candidate of

materials for immobilization or detection of biomolecules with phosphate groups.[40] Similar studies have demonstrated adsorption of DNA via phosphate groups[41-43] or immobilization of laccase via enzyme carboxylate terminal groups onto the solid surface modified by Zr^{4+}.[43-46]

We have chosen Hg^{2+} as an incarnation of this new paradigm. It is well-known that Hg^{2+} as a poisonous heavy metal ion, could easily accumulate in organisms and cause irreversible damage to the health of human being, such as damage DNA[47], inhibit ligand–receptor interactions[48], disable normal functions of the liver and kidney[49], disrupt the immune system homeostasis[50] and even lead to death. Thus, a convenient and fast method to detect Hg^{2+} is of great importance for the health of human beings. Recently, researchers have developed several kinds of Hg^{2+} sensor based on nanoparticles[36,51], DNAzymes[34,35,52], proteins[53], organic chromophores[54] or fluorophores[39,55,56] and quantum dots[36,57,58]. Through these methods have contributed to the detection of Hg^{2+}, most of them have some limitations due to the sophisticated synthesis of probe materials, tedious steps for functionalization or poor selectivity with interference from closely related metal ion. The combination of asymmetrical nanopore with SWNTs can contribute to addressing these challenges.

2 Experimental section

2.1 Materials

PET (polyethylene terephthalate) membranes (diameter =3 cm, thickness = 12 μm) that had been irradiated with a heavy ion of 2.2 GeV kinetic energy to create a single damage track through the membrane were obtained from GSI (Darmstadt, Germany).

Oligonucleotides (T-rich ssDNA: (5′-TTCTTTCTTCCCCTTGTTTGTT) was synthesized by Sangon Biotechnology Co., Ltd (Shanghai, China). Branched polyethyleneimine (PEI, MW=25000) was purchased from Sigma-Aldrich (St. Louis, MO, USA). Sodium hydroxide (NaOH) and potassium chloride (KCl) were purchased from Beijing Chemical Reagent Company (Beijing, China). All of the chemicals were at least analytical grade. The water used throughout all experiments was purified by a Milli-Q system (Millipore, Bedford, MA, USA). The stock solution of $Zr(CH_3COO)_4$ (15-16%wt) was obtained from Aladdin (Beijing, China). The stock solution of $Hg(CH_3COO)_2$ (10 mM) and other metal ion stock solutions (10 mM) were prepared in MilliQ water, and 10 mM Tris-HCl buffer was also used for further dilution. The oligonucleotides were quantified using a Cary 50 Scan UV-visible spectrophotometer (Varian, USA), lyophilized and kept at -20℃, and dissolved in 10 mM Tris-HCl buffer (KCl 100 mM, pH= 7.4) as stock solutions.

2.2 Preparation of asymmetrical single pore and cylindrical multipores

Each side of the PET membrane was treated with UV light (4 mW/cm^2) for one hour allows the activation of the polymer foil. Polymer membrane was sandwiched between two half compartments each of which contained etching solution (6 M NaOH) and stopping solution (1 M HCOOH plus surfactant 2A1), respectively and the etching temperature was maintained at 40℃. The whole etching process was controlled by monitoring current through the membrane across which one volt potential difference was applied. The current remained zero as long as the pore did not break through. The current after the breakthrough can be monitored via a picoammeter/voltage source

(Keithley 6487, Keithley Instruments, Cleveland, OH) and when the desired current was reached, the etching process was stopped by replacing the etching solution with the stopping solution to neutralize the etching solution in the pore. After chemical etching, the membranes were thoroughly washed with purified water and dried under nitrogen flow. The image of the base side of the conical pore in the polymer membrane were obtained with field-emission scanning electron microscopy (ESEM XL-30) by using multipores instead of single pore, the image was shown in Figure 1, the diameter of the base opening corresponding to the average value of 20 pores in the same membrane, if not specifically noted. The diameter of the tip opening was calculated by the following equation:

$$d = 4LI/\pi D\kappa V \quad (1)$$

Where I/V is the slope of the current-versus-voltage, L is the thickness of the membrane after etching, κ is the ionic conductivity of measuring solution, d is the diameter of tip opening and D is the diameter of base opening.

By immersing the PET membrane with multi-tracks into 2 M NaOH at 65℃ for half an hour, cylindrical multipores were formed, the image were presented in Figure S1. After modified with PEI and Zr^{4+}, XPS was applied for further characterization.

2.3 Functionalization with PEI and zirconium

The carboxylic (-COOH) groups generated on the channel surface during the track-etching process were functionalized with PEI by the following procedure. 1 mL of PEI (1 mg/ml) aqueous solution was placed on the tip of the track-etched polymer membrane, and allowed to self-assemble for 4 h. After the adsorption of PEI, the

membrane was washed with distilled water three times, and to determine the success of the adsorption by the I–V curves. After the above procedures, the PEI-modified asymmetrical nanopore was immersed in Zr^{4+} solution (4%wt) for 2h, then the Zr^{4+}-PEI modified asymmetrical nanopore was dried under vacuum at room temperature for following metal ions measurement. Same procedure was used for the chemical modification of multi-channel membranes, which was used for XPS characterization.

2.4 Current-versus-voltage measurements and X-ray photoelectron spectroscopy characterization

The prepared membrane with asymmetrical nanopore inside was sandwiched between two half components filled with conductive electrolyte in order to measure the I-V curve. For measurement of tip opening, both halves of the cell were filled with sodium phosphate solution (100 mM, 1 M KCl and pH=3.0). A pair of Ag/AgCl electrodes was placed into each half-cell solution, and a picoammeter/voltage source was used to apply the desired transmembrane potential, and measure the ionic current across the single pore membrane.

XPS analysis was utilized to confirm the PEI, Zr^{4+} and T-rich ssDNA were immobilized on PET surface. XPS data were obtained with an ESCALab250i-XL electron spectrometer from VG Scientific using 300 W Al Kα radiations.

3 Results and discussion

3.1 Design principle of nanopore-based ion sensor

Scheme 1 represents the schematic illustration of detection mechanism. The presence of

Hg^{2+} induces the folding of thymine -rich ssDNA with the formation of thymine-Hg^{2+}-thymine (T-Hg^{2+}-T).[56,59,60] As with other aptamers with compact structure, the folded DNA with metal ion-mediated T-Hg^{2+}-T base pair also shows low inclination to interact with SWNTs.[16,39] Instead, the folded DNA can be easily accumulated on the nanopore surface via the Zr^{4+}-PO_4^{3-} interaction. Before the DNA adsorption, the nanopore coated with Zr^{4+}-PEI is positively charged. Whereas high negatively charged DNA can neutralize the surface charge of the nanopore. The change in the surface charge of the nanopore can be monitored by I-V curves.

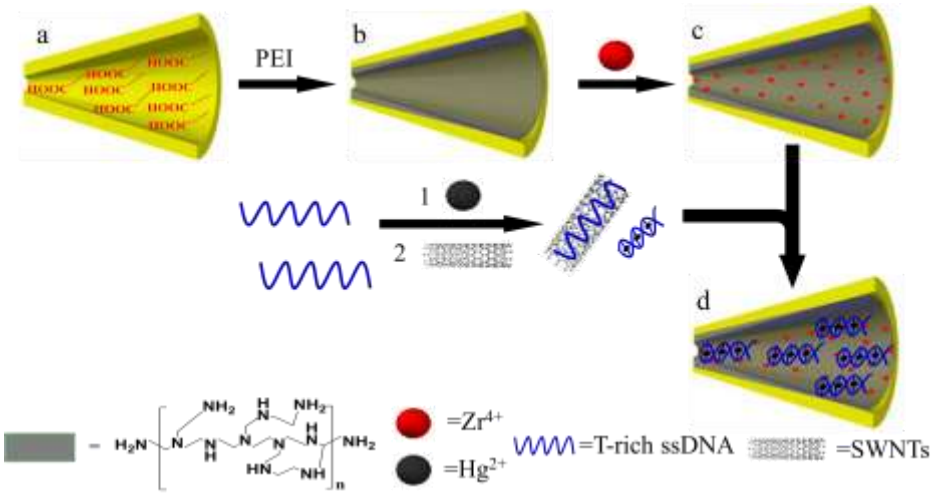

Scheme 1. Schematic illustration of the sensing strategy based on Zr^{4+}-PEI modified single nanopore. (a) A cone-shaped nanopore with abundant carboxyl groups on the surface. (b) Electrostatic adsorption of PEI onto the nanopore. (c) Adsorption of Zr^{4+} onto the PEI-coated nanopore. (d) Counting of Hg^{2+}-folded duplex DNA via the nanopore. The SWNTs remove the excess ssDNA.

3.2 Characterization of the nanopore biosensor

Each step in the assembling process can be confirmed with I-V curves obtained by

scanning the transmembrane potential. As shown in Figure 2, after electrostatic adsorption of branched polyethyleneimine (PEI), a distinct upward I-V curve was observed, which is in sharp contrast to the downward I-V curve with nascent nanopore. The further coating of Zr^{4+} slightly enhanced the ion current rectification, which is reasonable and expected since the Zr^{4+} is positively charged. The successful coating was further validated by X-ray photoelectron spectroscopy (XPS) characterization (Figure 2B). The peaks unique to $3d_{3/2}$ and $3d_{5/3}$ of Zr^{4+} were clearly observed in the XPS. The addition of Hg^{2+}-mediated duplex DNA significantly suppressed the ion current rectification (orange curve, Figure 2). All unfolded DNA were removed by SWNTs, precluding any possibility of interference. The Zr^{4+} plays a very important role in the adsorption of DNA. The data in Figure S3 shows that without the existence of Zr^{4+} on the nanopore surface, the I-V curves showed negligible change in the ion current rectification upon adjusting the concentration of Hg^{2+} from 0 to 3 μM while keeping ssDNA and SWNTs concentration constant.

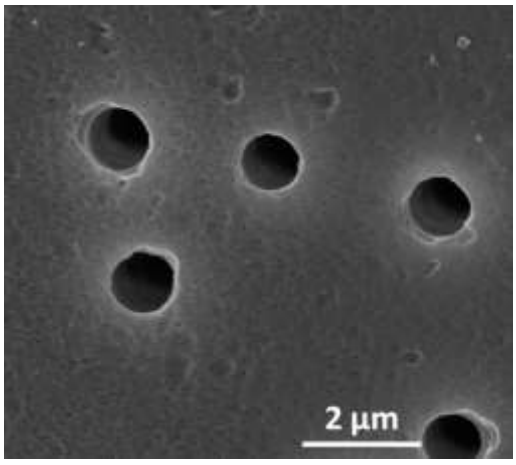

Figure 1. Scanning electron microscopy (SEM) of the base side of the conical nanopores in a PET membrane which is etched under the same conditions for single

pore. The diameter of the base opening is about 1100 nm, and the tip diameter of the single nanopore is calculated to be 53 nm.

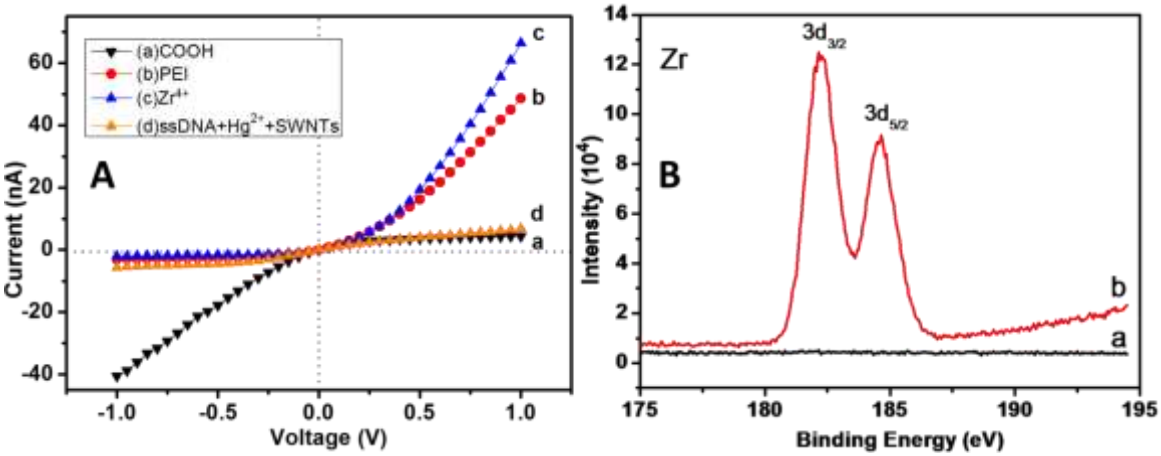

Figure 2. (A) I-V characteristics of the assembling processes within the nanopore. (a), (b), (c) and (d) represent nascent nanopore, PEI coating, Zr^{4+} adsorption and adsorption of Hg^{2+}-induced DNA duplex, respectively. (B) XPS characterization of multi-nanopores before (a) and after (b) modified with Zr^{4+}-PEI.

3.3 Performance of Hg^{2+} detection

The working solution containing the T-rich ssDNA was obtained by diluting the stock solution to 200 nM using 10 mM Tris-HCl buffer (100 mM KCl, pH=7.4). For Hg^{2+} assays, 100 μL of the T-rich ssDNA and appropriate concentration of Hg^{2+} solution mixed for 30 min. Then, the SWNTs solution was mixed and incubated for 20 min at room temperature[37] (final concentration: T-rich ssDNA 200 nM, SWNTs 50 μgL^{-1}). Finally, the I-V curves were measured.

We used the Langmuir adsorption equation to analyze the current data, according to Equation (2) and (3)[14,15]:

$$\theta = \frac{KC}{1+KC} \quad (2)$$

where θ is the fractional coverage of the molecule on the surface, K is the binding constant with units of $Lmol^{-1}$ and C is the concentration of the Hg^{2+} in the contacting solution phase. θ is also given by:

$$\theta = \frac{I_0 - I_i}{I_0 - I_{\min}} \quad (3)$$

where I_0 is the current obtained in the absence of Hg^{2+}, I_i is the current observed at an intermediate Hg^{2+} concentration, and I_{min} is the current that the surface adsorption reached the maximum capacity.

We used the current data at +1 V, and a series of θ was obtained. The plot of surface coverage (θ) versus concentration of Hg^{2+} was shown in Figure 3B and Figure 5B, and the experimental data was best fit the Equation (2).

3.4 Sensitivity of the nanopore biosensor for Hg(II) detection

Sensitivity are very important issues for the Zr^{4+}-PEI modified nanochannel Hg^{2+} sensor. In order to test the sensitivity of the Zr^{4+}-PEI coated nanopore, various concentrations of ssDNA were spiked into the solution chamber on the one side of the membrane containing the tip opening. 10 minutes of accumulation which was implemented by scanning transmembrane potential between ±1 V was acquired to improve the sensitivity. The 10 nM concentration of ssDNA can induce significant decrease of ion current rectification (Figure S4A, Supporting Information). Concentration above 100 nM is ready to saturate the nanopore surface around tip opening, which was reflected by the plot of surface coverage versus DNA concentration

(Figure S4B).

With the assistance of SWNTs, the influence of ssDNA can be fully removed, which was confirmed by the almost overlapping of the black curve and the red curve in Figure 3A. The black and red curves for Zr^{4+}-PEI coated nanopore were measured in only buffer and buffer containing ssDNA+SWNTs, respectively. Along with the gradual increase of the Hg^{2+} concentration, the I-V curves showed the corresponding changes until the I-V curve showed no more shift. Concentration of Hg^{2+} above 500 nM can allow the saturation of the nanopore surface. The surface absorption of Hg^{2+} adhered to the Langmuir adsorption model as presented in Figure 3B. The surface coverage (θ) plotted as the function of Hg^{2+} concentration showed linear relationship with Hg^{2+} concentration below 100 nM. The limit of detection (LOD) is defined as the concentration corresponding to the surface coverage at three times standard deviation of blank without analyte was 8.3 nM, which is lower than the toxicity level of Hg^{2+} in drinking water (30 nM) defined by Word Health Organization (WHO).

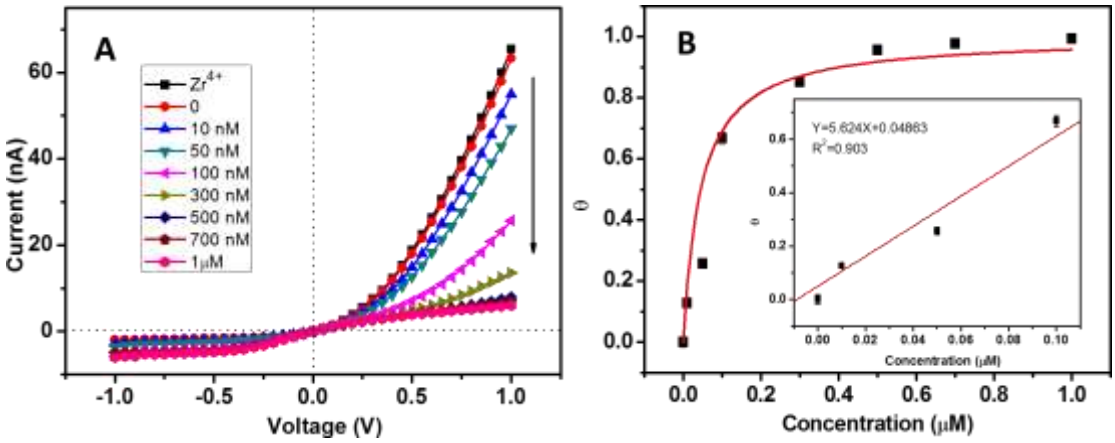

Figure 3. (A) I-V curves for Zr^{4+}-PEI modified conically shaped nanopore in the presence of various concentrations of Hg^{2+}. (B) Plot of surface coverage (θ) versus concentration of Hg^{2+}. The inset displays the linear response between θ and the

concentrations of Hg^{2+} ranging from 0 nM to 100 nM. The error bars were obtained from three replicate measurements.

3.5 Selectivity of nanopore in combination with SWNTs

Just as externally functionalized nanopore can provide selectivity toward the target of interest, the selectivity of the biomimetic nanopore sensor for Hg^{2+} detection was also investigated in combination with SWNTs. We chose a variety of environmental relevant metal ions, including Ca^{2+}, Mg^{2+}, Ni^{2+}, Mn^{2+}, Pb^{2+}, Ba^{2+}, Co^{2+}, Zn^{2+}, Fe^{3+}, Cd^{2+}, Cu^{2+} were used for evaluating the selectivity of the biomimetic sensor for Hg^{2+}. Figure S5A shows the I-V curves upon exposure of the biomimetic nanopore sensor to all the above metal ions. The presence of Hg^{2+} ions in the background electrolyte resulted in a drastic decrease in the ion flux across the nanochannel, whereas the current stayed nearly unchanged in the presence of the other tested ions. The result shows that the biomimetic nanopore exhibits selectivity for Hg^{2+} ions. The current change (ΔI) at +1 V was determined to quantify the changes in the ionic current passing though the modified nanochannels upon exposure to different metal ions. From the current change data (Figure 4), it is clearly indicated that the biomimetic nanopore sensor displayed high selectivity for Hg^{2+} and this approach has potential for future use.

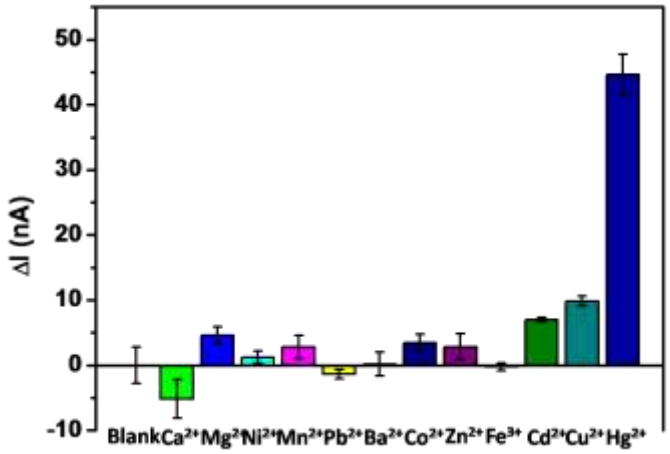

Figure 4. Selectivity of the Zr^{4+}-PEI modified single nanopore in combination with SWNTs. The concentration of each ion is 1 μM and the Current change (ΔI) for each ion is measured at +1V. All measuremnts were done in 10 mM Tris-HCl buffer (100 mM KCl, pH=7.4, 200 nM ssDNA).

3.6 Application of the nanopore biosensor

We tested the applicability of our biomimetic nanopore sensor for Hg^{2+} detection in lake water (Nan Lake in Changchun). The same procedure as that for measurement in buffering solution was applied. A series of Hg^{2+} solution are prepared by spiking different amount of Hg^{2+} into 100-fold diluted lake water. The corresponding I-V curves are presented in Figure 5A and the plot of surface coverage (θ) versus concentration of Hg^{2+} is shown in Figure 5B. Together with the recovery analysis (Table 1), these results show the similar trend to those for pure buffering solution and we confirmed that our proposed method can be used in real samples detection.

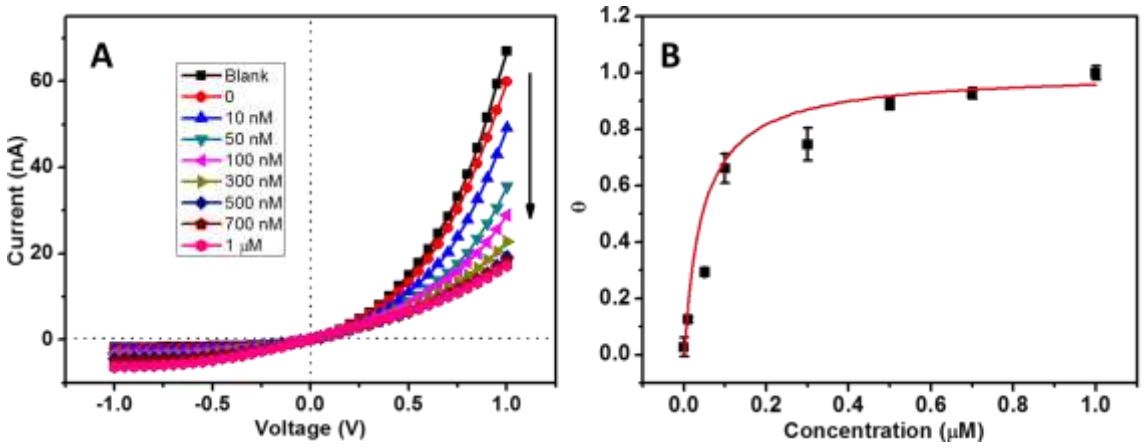

Figure 5. (A) I-V characteristics of Zr^{4+}-PEI modified conically shaped nanopore upon addition of various concentration of Hg^{2+} from 0 to 1μM into 100-fold diluted lake water with buffering solution (10 mM Tris-HCl , 100 mM KCl, pH=7.4）. (B) Plot of surface coverage (theta) versus concentration of Hg^{2+}. The error bars were obtained from three replicate measurements. Experimental conditions: 10 mM Tris-HCl (100 mM KCl, pH=7.4), 200 nM ssDNA and 50 μgL^{-1}SWNTs.

Table 1. Analytical results for Hg^{2+} in lake water

Sample	Added (nM)	Found (nM)	Recovery (%)
Lake Water	0	ND[a]	
	10	13.4±0.6	134±6.0
	50	43.5±4.0	87±8.0
	100	108.9±9.3	98±9.3

[a]ND stands for not detection.

4 Conclusions

In summary, a new direction in biosensor based on cone-shaped nanopore is proposed. By combination with other nanomaterials such as SWNTs, sensitivity and selectivity of biomimetic nanopore can be individually addressed. The successful achievement of this goal is also reliant on the coating of Zr^{4+} on the cone-shaped nanopore with good reproducibility and strong affinity toward DNA. The aversion of probe immobilization on the nanopore is one of the unique features of this strategy, which should not be

restricted to the detection of Hg^{2+} and the utilization of SWNTs. Considering that a slew of aptamers have been involved in construction of various biosensing platforms, there should be large space for future development in this new direction. It can be envisioned that next effort to integrate signal amplification into this new system will pour more stimuluses into the development of the nanopore field.

Acknowledgments

This work was supported by National Natural Science Foundation of China (No. 21275137), Start Funding from Changchun Institute of Applied Chemistry (CAS) and Supporting Funding for Creative Young Scientist (CAS).

References

1 X. Hou, W. Guo and L. Jiang, *Chem. Soc. Rev.*, 2011, **40**, 2385.

2 C. Ho, R. Qiao, J. B. Heng, A. Chatterjee, R. J. Timp, N. R. Aluru and G. Timp, *Proc. Natl. Acad. Sci. USA*, 2005, **102**, 10445.

3 B. N. Miles, A. P. Ivanov, K. A. Wilson, F. Dogan, D. Japrung and J. B. Edel, *Chem. Soc. Rev.*, 2013, **42**, 15.

4 H. Zhang, Y. Tian and L. Jiang, *Chem. Commun.*, 2013, **49**, 10048.

5 C. Han, H. Su, Z. Sun, L. Wen, D. Tian, K. Xu, J. Hu, A. Wang, H. Li and L. Jiang, *Chem. Eur. J.*, 2013, **19**, 9388.

6 L. T. Sexton, L. P. Horne, S. A. Sherrill, G. W. Bishop, L. A. Baker, C. R. Martin, *J. Am. Chem. Soc.*, 2007, **129**, 13144.

7 L. T. Sexton, H. Mukaibo, P. Katira, H. Hess, S. A. Sherrill, L. P. Horne and C. R. Martin, *J. Am. Chem. Soc.,* 2010, **132**, 6755.

8 Z. S. Siwy, *Adv. Funct. Mater.,* 2006, **16**, 735.

9 D. Momotenko and H. H. Girault, *J. Am. Chem. Soc.,* 2011, **133,** 14496.

10 Z. Siwy, E. Heins, C. C. Harrell, P. Kohli, and C. R. Martin, *J. Am. Chem. Soc*., **2004**, **126**, 10850.

11 S. Liu, Y. Dong, W. Zhao, X. Xie, T. Ji, X. Yin, Y. Liu, Z. Liang, D. Momotenko, D. Liang, H. H. Girault and Y. Shao, *Anal. Chem.,* 2012, **84**, 5565.

12 M. Ali, M. N. Tahir, Z. Siwy, R. Neumann, W. Tremel and W. Ensinger, *Anal. Chem.,* 2011, **83**, 1673.

13 J. H. Wang and C. R. Martin, *Nanomedicine*, 2008, **3**, 13.

14 Z. Guo, J. Wang and E. Wang, *Talanta*, 2012, **89**, 253.

15 L. Wen, Z. Sun, C. Han, B. Imene, D. Tian, H. Li and L. Jiang, *Chem. Eur. J.*, 2013, **19**, 7686.

16 W. J. Zhang, Z. Y. Meng, J. L. Zhai, and P. Heng, *Chem. Commun.*, 2014, DOI: 10.1039/C3CC47999D.

17 J. A. Cracknell, D. Japrung and H. Bayley, *Nano lett.*, 2013, **13**, 2500.

18 Y. He, M. Tsutsui, R. H. Scheicher, F. Bai, M. Taniguchi and T. Kawai, *ACS nano,* 2013, **7**, 538.

19 S. W. Kowalczyk, M. W. Tuijtel, S. P. Donkers and C. Dekker, *Nano lett.*, 2010, **10**, 1414.

20 M. Ali, S. Nasir, Q. H. Nguyen, J. K. Sahoo, M. N. Tahir, W. Tremel and W. Ensinger, *J. Am. Chem. Soc.,* 2011, **133**, 17307.

21 M. Ali, S. Nasir, P. Ramirez, J. Cervera, S. Mafe and W. Ensinger, *J. Phys. Chem. C*, 2013, **117**, 18234.

22 M. Ali, Q. H. Nguyen, R. Neumann and W. Ensinger, *Chem. Commun.*, 2010, **46**, 6690.

23 M. Ali, P. Ramirez, M. N. Tahir, S. Mafe, Z. Siwy, R. Neumann, W. Tremel and W. Ensinger, *Nanoscale*, 2011, **3**, 1894.

24 C. Han, X. Hou, H. Zhang, W. Guo, H. Li and L. Jiang, *J. Am. Chem. Soc.,* 2011, **133**, 7644.

25 L. D. Li, X. J. Mu, Y. Peng, Z. B. Chen, L. Guo and L. Jiang, *Anal. Chem.*, 2012, **84**, 10554.

26 L. Lin, Y. Liu, J. Yan, X. Wang and J. Li, *Anal. Chem.*, **2013**, *85*, 334-340.

27 N. Liu, Y. Jiang, Y. Zhou, F. Xia, W. Guo and L. Jiang, *Angew. Chem. Int. Ed.*, **2013**, *52*, 2007-2011.

28 C. Zhao, X. Li, L. Li, X. Gong, Y. Chang and J. Zheng, *Chem. Commun.*, 2013, **49**, 9317.

29 Y. Tian, Z. Zhang, L. Wen, J. Ma, Y. Zhang, W. Liu, J. Zhai and L. Jiang, *Chem. Commun.*, 2013, **49**, 10679.

30 Y. Tian, X. Hou, L. Wen, W. Guo, Y. Song, H. Sun, Y. Wang, L. Jiang and D. Zhu, *Chem. Commun.*, 2010, **46**, 1682.

31 I. Vlassiouk, T. R. Kozel and Z. S. Siwy, *J. Am. Chem. Soc.*, 2009, **131**, 8211.

32 Z. S. Siwy, M. R. Powell, Petrov, E. Trautmann C. A. Kalman,and R. S. Eisenberg, *Nano Lett.*, 2006, **6**, 1729.

33 Z. Guo, J. Wang, J. Ren and E. Wang, *Nanoscale*, 2011, **3**, 3767.

34 Y. Hao, Q. Guo, H. Wu, L. Guo, L. Zhong, J. Wang, T. Lin, F. Fu and G. Chen, *Biosens. Bioelectron.*, 2014, **52**, 261.

35 X. Lou, T. Zhao, R. Liu, J. Ma and Y. Xiao, *Anal. Chem.*, 2013, **85**, 7574.

36 J. L. MacLean, K. Morishita and J. Liu, *Biosens. Bioelectron.*, 2013, **48**, 82.

37 Z. Guo, J. Ren, J. Wang and E. Wang, *Talanta*, 2011, **85**, 2517.

38 L. Zhang, H. Wei, J. Li, T. Li, D. Li, Y. Li and E. Wang, *Biosens. Bioelectron.*, 2010, **25,** 1897.

39 L. Zhang, T. Li, B. Li, J. Li and E. Wang, *Chem. Commun.*, 2010, **46**, 1476.

40 R. K. Shervedani and S. Pourbeyram, *Biosens. Bioelectron.*, 2009, **24**, 2199.

41 S. Q. Liu, J. J. Xu and H. Y. Chen, *Colloids Surf. B*, 2004, **36**, 155.

42 J. Wang, F. Wang, Z. Xu, Y. Wang and S. Dong, *Talanta*, 2007, **74**, 104.

43 C. Fang, H. Ji, W. Y. Karen and S. R. Rafei, *Biosens. Bioelectron.*, 2011, **26**, 2670.

44 C. Fang, A. Agarwal, K. D. Buddharaju, N. M. Khalid, S. M. Salim, E. Widjaja, M. V. Garland, N. Balasubramanian and D. L. Kwong, *Biosens. Bioelectron.*, 2008, **24**, 216.

45 H. M. Meng, T. Fu, X. B. Zhang, N. N. Wang, W. Tan, G. L. Shen and R. Q. Yu, *Anal. Chem.*, 2012, **84**, 2124.

46 W. Qi, J. Zhao, W. Zhang, Z. Liu, M. Xu, S. Anjum, S. Majeed and G. Xu, *Anal. Chim. Acta*, 2013, **787**, 126.

47 A. Renzoni, F. Zino and E. Franchi, *Environ. Res.*, 1998, **77**, 68.

48 N. Basu, M. Kwan and H. M. Chan, *J. Toxicol. Env. Heal., A*, 2006, **69**, 1133.

49 X. Liu, Y. Tang, L. Wang, J. Zhang, S. Song, C. Fan and S. Wang, *Adv. Mater.*, 2007, **19,** 1471.

50 S. E. Ziemba, R. R. Mattingly, M. J. McCabe and A. J. Rosenspire, *Toxicol. Sci.*, 2006, **89**, 145.

51 J. Zhao, B. Zhu, H. Yu, L. Yan, Q. Wei and B. Du, *J. Colloid Interface Sci.,* 2013, **389**, 46.

52 Y. Zhang, H. Zhao, Z. Wu, Y. Xue, X. Zhang, Y. He, X. Li and Z. Yuan, *Biosens. Bioelectron.,* 2013, **48**, 180.

53 P. Chen,and C. A. He, *J. Am. Chem. Soc.*, 2004, **126**, 728.

54 X. Cheng, Q. Li, C. Li, J. Qin and Z. Li, *Chem. Eur. J.*, 2011, **17**, 7276.

55 G. F. Wang, G. Xu, Y. H. Zhu and X. J. Zhang, *Chem. Commun.*, 2014, **50**, 747.

56 M. Li, X. Zhou, W. Ding, S. Guo and N. Wu, *Biosens. Bioelectron.*, 2013, **41**, 889.

57 W. Guo, J. Yuan and E. Wang, *Chem. Commun.*, 2009, **69**, 3395.

58 J. Ma, Y. Chen, Z. Hou, W. Jiang and L. Wang, *Biosens. Bioelectron.*, 2013, **43**, 84.

59 M. Zhang, H. N. Le, X. Q. Jiang and B. C. Ye, *Chem. Commun.*, 2013, **49**, 2133.

60 F. Xuan, X. Luo and I. M. Hsing, *Anal. Chem.*, 2013, **85**, 4586.